5. RF PHOTOCATHODE GUN

OVERVIEW

The proposed facility requires a high brightness electron beam with an exceptionally low vertical emittance to produce, through beam manipulation and x-ray optics, hard x-ray photon pulses with pulse length of tens of femtoseconds. These requirements are satisfied by a laser-excited, photoemissive electron source, the photoinjector, with the photocathode residing in a high-gradient rf cavity, followed immediately by a short accelerator section to bring the beam up to the 10 MeV range. Generation of low vertical emittance downstream is accomplished by a combination of a finite solenoid magnetic field at the cathode surface and a short skew quadrupole lattice situated downstream from the exit of the rf gun. Table 5-1 lists the parameters required of the flat beam injector.

Table 5-1 Flat Beam Injector Parameters

Electron beam parameters at injector exit:		
Energy	10	MeV
Charge	1-3	nC
Normalized RMS horizontal emittance	~20	mm-mrad
Normalized RMS vertical emittance @ 1 nC	<0.4	mm-mrad
Energy spread at 10 MeV	±15	keV
Pulse length (uniform distribution)	20	ps
Repetition rate	~10+	kHz
RF gun parameters:		
RF frequency	1.3	GHz
Peak electric field on a cathode	~ 64	MV/m
Normalized geometric emittance at 1 nC	3	mm-mrad
Laser parameters:		
Wavelength (4^{th} harmonic of Nd:YLF laser)	267	nm
UV pulse energy at cathode	~10	μJ
Pulse length (FWHM)	20+	ps

The flat beam photoinjector is composed of two main sections: the rf gun with integrated photocathode, and the flat beam adapter including several skew quadrupoles. A schematic of the injector is shown in Figure 5-1. The ~0.5-m long rf gun is followed by a short (~30-40 cm) drift section, and then the ~1.5-m long adapter section.

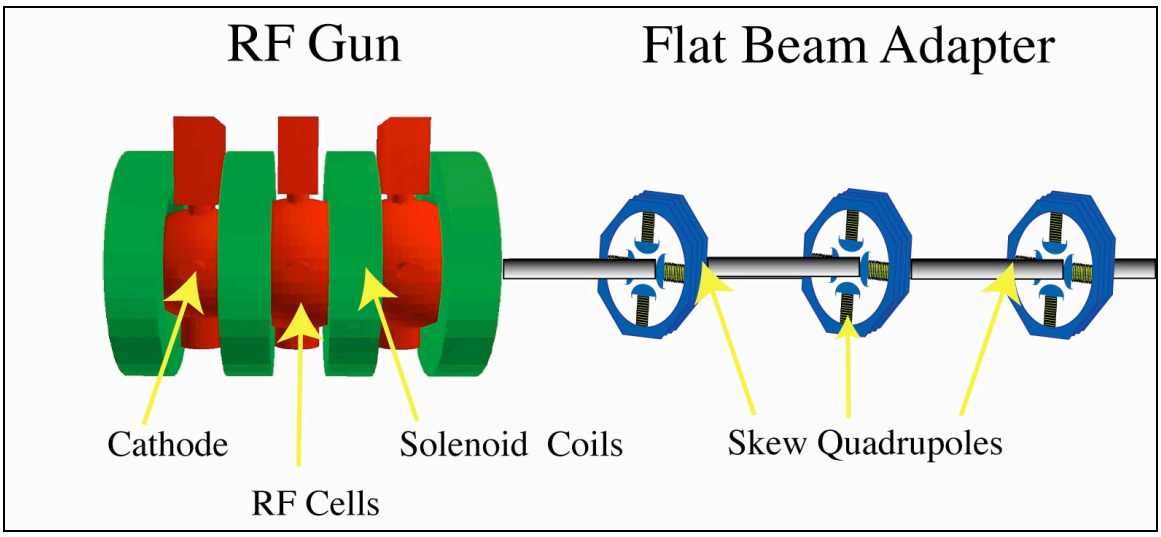

Figure 5-1 Flat beam injector beamline.

Technical Issues for Photoinjectors

There are difficult technical issues resulting from both the beam requirements tabulated above as well as the operational requirements of high duty factor and low maintenance required of a user facility. We discuss here, issues common to all high brightness photoinjectors, specific issues for flat beam production and transport, and issues relating to high duty factor operation.

Generic issues for high brightness electron beam production

The electron beam is generated when an intense laser pulse strikes a photocathode. The surface work function of the material defines the necessary laser frequency with which to liberate the electrons. These electrons scatter from the surface to the vacuum region adjacent to the cathode within the first rf cavity. At this point, they are captured by the rf field in the cavity and accelerated. By properly matching the rf cavity phase with the arrival time of the laser pulse, the liberated electrons are captured, accelerated, and passed on to subsequent accelerating cells.

The quantum efficiency (Q.E.) of the photoemissive cathode is the ratio of the number of emitted electrons to the number of incident photons. For various photocathode materials the Q.E varies from $<10^{-4}$ for copper to ~0.10 for GaAs(Cs,O) (see Table 5-2). To produce an electron beam with charge Q_{bunch} from a photocathode requires a laser pulse capable of delivering energy

Table 5-2 Summary of commonly used photocathode materials

Material	Q.E. Range (%)	λ (nm)	Lifetime	Vacuum Required (Torr)
Metal (Cu)	0.02-0.06	260	Months	10^{-7}
CsK_2Sb	~ 5	527	-	10^{-10}
Cs_2Te	1 - 5	260	Months	10^{-9}
LaB_6	~ 0.1	355	Months	10^{-7}
GaAs(Cs,O)	~ 10	527	Days	10^{-11}

$$W_{laser} = \frac{Q_{bunch}}{Q.E.} \frac{hc/e}{\lambda_{laser}}, \tag{1}$$

where hc/e is 1.24 μJ-nm/nC. With a laser wavelength of 0.267 μm (4.64 eV) to match the work function of the Cs_2Te surface, this energy is approximately 0.5 μJ per pulse to produce a 1 nC bunch with a cathode Q.E. of 1%. Operational requirements may push toward production of beams with 3 nC per bunch, or even higher charge. Also, over time, the Q.E. of the photocathode may droop, requiring even larger laser pulse energies to be delivered to the cathode. For these reasons, the laser system is specified to deliver ~10 μJ pulse.

Laser systems can routinely (even easily) deliver this energy in a single pulse to a photocathode surface. One challenge, however, is to operate these lasers at 10 kHz and above. Thermal loading effects on the optics and amplifier media must be controlled to maintain stability and beam quality.

From the standpoint of beam dynamics and user operations, the laser must display short-term and long-term stability in its operation. Of greatest concern is the spatial-temporal distribution of the laser pulse at the cathode surface. The laser must deliver an illumination onto the cathode that is uniformly distributed in the transverse plane, as well as uniform in time along the pulse. Any deviations will induce non-uniformities in the electron beam distribution that can drive emittance growth downstream. Laser pulse shaping techniques in both the transverse and longitudinal dimensions are currently under development [1,2].

In addition to the laser, the photocathode must display uniform emission under optimal (uniform) illumination. The local distribution of quantum efficiency on the cathode surface must be uniform to produce a uniform beam. Thermal emittance characteristics of photocathode materials depend on the laser wavelength, angle of incidence, surface treatment and vacuum, and surface temperature. At present, understanding of the limiting effects on thermal emittance is only at a rudimentary level. There has been some theoretical work, but almost no experimental measurements. Work is underway at various laboratories [3,4] to quantify the thermal emittance characteristics of various photocathode materials.

The vacuum requirements on coated photocathodes are severe, lest they display significant degradation in their quantum efficiency. They are typically prepared by sputtering onto a molybdenum substrate, which can then be stored for months in ultra-high vacuum (~10^{-11} torr) with little degradation of the surface work function and quantum efficiency. For optimal

performance, cesium-telluride photocathodes must be operated in a vacuum of ~10^{-9} torr. Operationally, cesium-telluride cathodes are known to degrade over a period of several months, with the quantum efficiency dropping from ~5-10% to ~0.5-1%. The initial quantum efficiency can often be recovered by UV treatment of the surface [5].

The use of Cs_2Te photocathodes in rf guns is relatively mature, and provides a useful set of parameters to create a working point design for the injector and ancillary drive laser system. It is not, however, the only available material. We will continue study into the use of alternative photocathode materials in order to ascertain the best choice, given our operating conditions of high duty factor, high brightness, and (relatively) low maintenance.

In a generic rf photoinjector the electron beam emittance is minimized by fast acceleration of the bunch to kinetic energies on the order of a few MeV. At this point, the beam may be transported for a short distance (~tens of cm to ~1 m) before suffering from excessive space charge induced blow up. External solenoid focusing is used to balance the space charge forces so that the beam is prepared for injection into the subsequent accelerator section. During acceleration, the influence of space charge on emittance blow-up rapidly diminishes as the beam energy increases. The emittance at the entrance to the injector linac is essentially *Frozen in*.

High brightness photoinjectors are characterized by their normalized peak brightness,

$$B_{peak} = \frac{I_{peak}}{\nu_4} = \frac{2I_{peak}}{\varepsilon_x \varepsilon_y} \tag{2}$$

where I_{peak} is the peak current carried by the beam, and the 4D rms transverse phase-space volume is characterized by the normalized rms emittances (ε_x and ε_y) via $\nu_4 = \varepsilon_x \varepsilon_y$. Figure 5-2 shows some recently constructed and commissioned photoinjectors, and the relation between peak brightness and operating rf frequency. The proposed flat beam photoinjector is added to the plot for comparison, and is seen to perform similarly to both the FNPL and TTF photoinjectors.

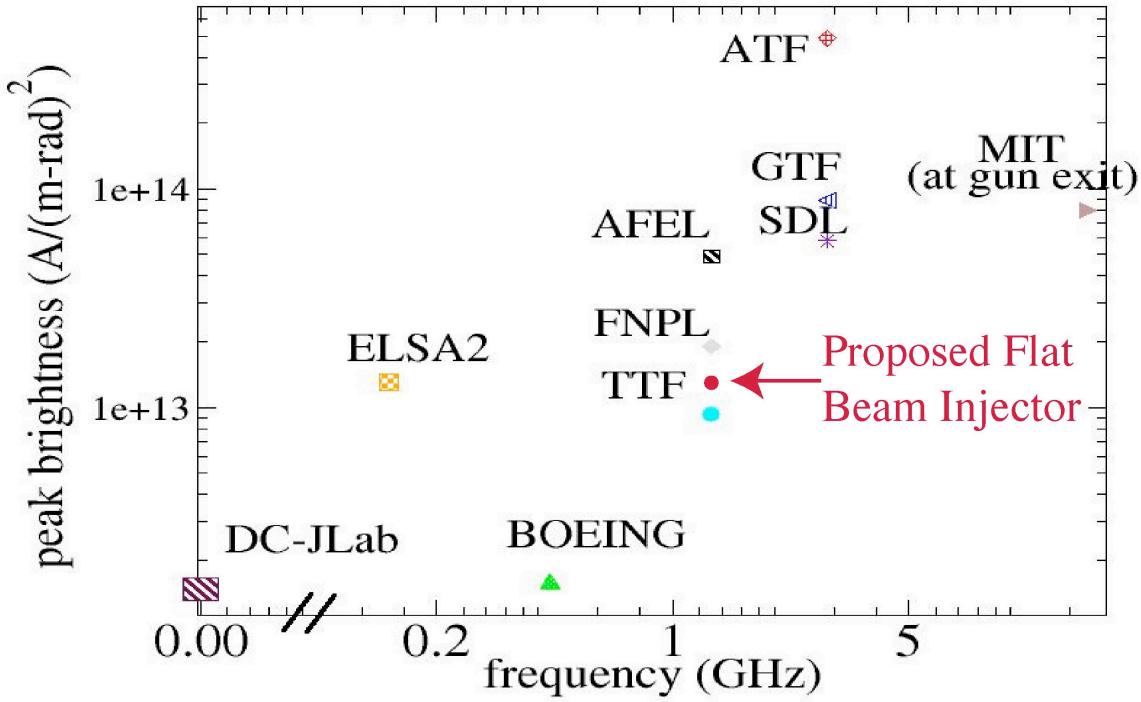

Figure 5-2 Measured peak brightness of recent photoinjectors. The proposed flat beam injector design brightness has been included for comparison. (Figure courtesy of P. Piot).

Specific issues for flat beam production

The flat beam photoinjector and transport scheme differs in some very important ways from the generic photoinjector described above. While this design shares the same issues as the generic case, it also brings in several new, specific issues.

In contrast to generic photoinjectors that employ reversed-polarity solenoids (bucking coils) to negate any residual magnetic field at the cathode plane, the generation of a flat beam through electron optics begins with the imposition of a strong solenoidal magnetic field at the photocathode. This will produce the necessary correlation between the horizontal and vertical phase spaces that ultimately results in a large emittance ratio. However, the presence of a large magnetic field at the cathode significantly changes the beam optics through the rf gun and beyond.

Additionally, upon exit from the gun the beam must be carefully matched to the flat beam adapter beamline. This short beamline of skew quadrupoles transforms the correlated, 4-D transverse phase space of the beam into uncorrelated, 2-D sub-spaces with a large horizontal: vertical emittance ratio. To do so, the quadrupole lattice must produce specifically tailored betatron phase advances in the horizontal and vertical planes.

The flat beam must be transported with a conventional quadrupole lattice and matched into the bunch compressor and subsequent linac structure. Localized variations in the bunch density,

transverse and longitudinal profiles, and bunch-to-bunch charge fluctuations must be carefully handled to minimize emittance growth at all stages, particularly up to the entrance of the first linac.

Thermal management in the high duty factor rf gun and laser

The high repetition rate, 10 kHz or more, of the 20-psec beam pulse represents a low beam duty factor. However, the relatively long filling time of the cavity results in a 5% rf duty factor, with a correspondingly high wall power density. Careful thermal management of the photoinjector is necessary. The laser system must also be carefully designed to operate at such high duty factors, as previously mentioned.

This chapter and the following three chapters discuss the current design photoinjector and address our understanding of the issues involved in producing flat beams of large emittance ratio. The first section presents our current design for the rf gun, including calculations of electromagnetic mode structure and mechanical stress analysis from inductive heat loading, rf drive requirements, and the placement of focusing solenoids. The second section discusses beam dynamics within the rf gun, including space charge effects, the role of beam launch timing with respect to the rf phase, and the effect of offset phasing between the different rf gun cells. The third section examines the process of emittance compensation for angular momentum dominated beams. Theoretical tools to help understand compensation are discussed, followed by recent experimental results. The last section describes previous and current studies on the flat beam adapter optics. The basic process is described in detail followed by results from a proof-of-concept experiment. Finally, a preliminary design for the flat beam adapter to be used in the proposed injector is presented, with the results from simulation that demonstrate the required low vertical emittance.

RF GUN ELECTROMAGNETIC DESIGN

The photoinjector will comprise a high-gradient reentrant gun cell with a Cs_2Te photocathode producing a 20 psec bunch with a peak current in the 50 ampere range, followed immediately by a 3-cell π-mode acceleration structure accelerating the beam to 10 MeV. All the cavities will be independently driven and phased. Calculations are presented on the design and performance of the rf gun cavities using the electromagnetic codes SUPERFISH [6], MAFIA [7], and NSYS [8].

Figure 5-3 shows the overall layout of the four cells, the left-most cell containing the photocathode, generating and accelerating the 20 psec bunch to 2 MeV, followed by a 3-cell π- mode accelerating structure, bringing the beam energy to 10 MeV.

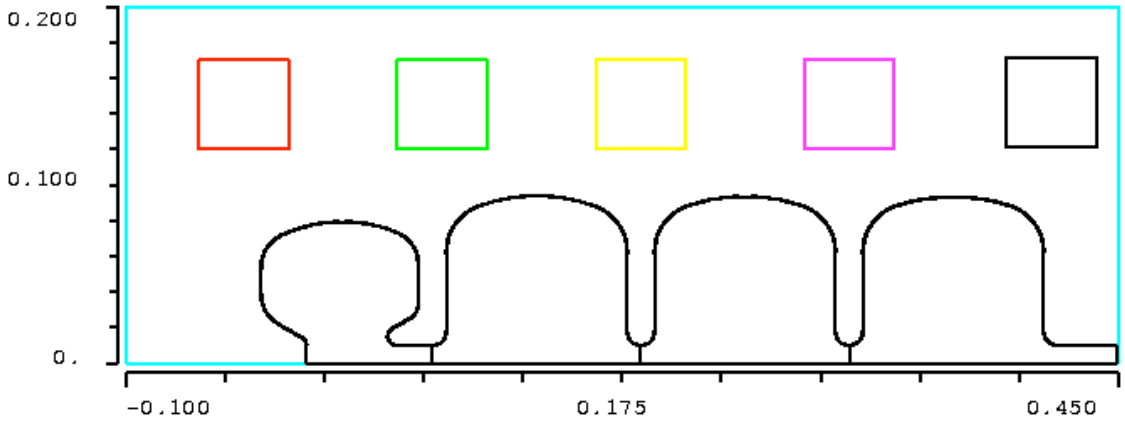

Figure 5-3 2-D model of rf gun cavities and solenoid magnets (MAFIA).

Solenoids surround the entire 4-cell structure, with waveguide couplers interposed between the separate windings. The longitudinal magnetic field at the cathode will be adjustable, to prepare the proper angular momentum of the launched beam for the flat beam transformer

The 1.3 GHz operating frequency is chosen as a compromise between surface power density and achievable electric field gradient. The 10 kHz repetition rate, folded with a 1/*e* cavity filling time of 3.4 microseconds with a loaded Q_L of approximately 10^4, requires that the cavity be overdriven to achieve full gradient in 5 microseconds. The cavity field variation during the 20-psecbeam pulse will be negligible, though pulse-to-pulse reproducibility is very important for timing stability.

Cell 1

The first cell is shaped to maximize both the beam energy at the end of the first cell and the field at the photocathode, while minimizing the peak electric field elsewhere in the cavity, minimizing the dark current, and reducing the tendency toward sparking. To minimize multipactoring and conditioning time, the walls of the cavity comprise sections of arcs, rather than parallel straight wall sections, used in former pillbox photoinjector configurations.

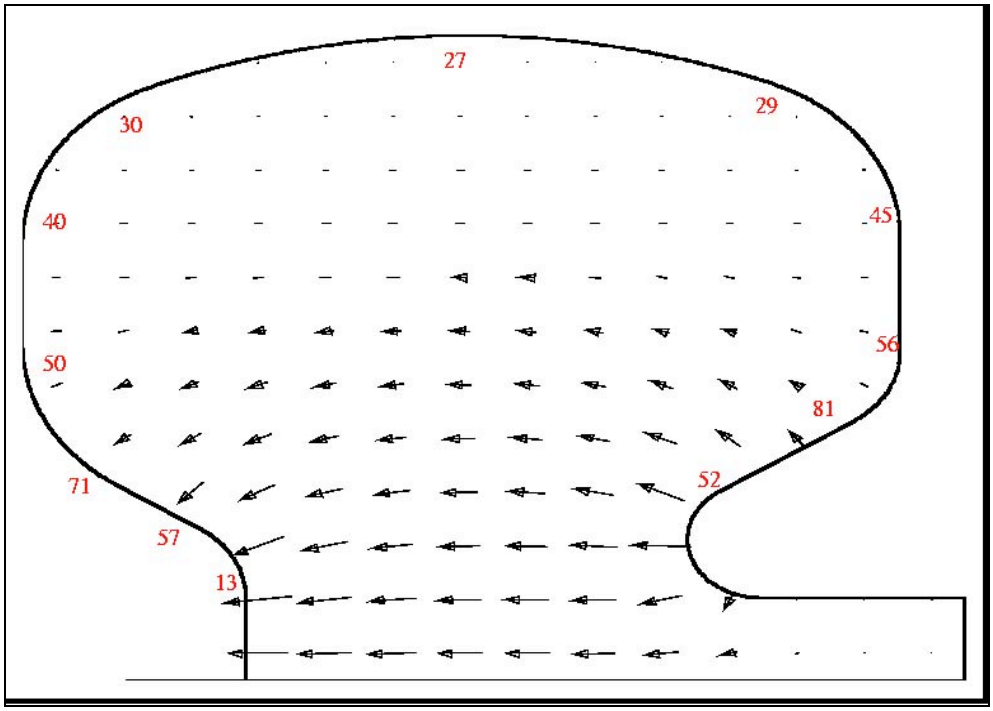

Figure 5-4 Cell-1 2-D geometry and accelerating mode electric field (SUPERFISH). The red numbers denote the corresponding average heat flux (W/cm^2) into the cavity at significant points.

Figure 5-4 shows the cavity outline, with the photocathode sited on a mesa, facing a reentrant nose-cone that increases the local field on the cathode surface and increases the shunt impedance of the cavity itself. The figure also shows the electric field lines for the 1.3 GHz fundamental mode. To achieve 64 MV/m electric field at the photocathode surface, 752 kW peak rf power is required. Beam loading is insignificant for a 1 nC, 20 psec beam pulse accelerated to 2 MeV. The extracted beam energy is ~2□millijoule where the stored energy in the cavity is 1.95 joule at operating gradient. Table 5-3 lists cathode cell parameters.

The peak azimuthal H-field over the rf pulse produces an RMS power dissipation in 100% steady-state operation of 2300 watts/cm^2, which, when operated at the drive power time dependence described below, becomes an RMS power dissipation of 81 watts/cm^2 in the upper part of the exit nosecone and much less elsewhere in the cavity. Integrated over the entire cavity, the average RMS thermal power dissipation is 38 watts/cm^2 at the peak of the rf pulse.

The long exit beampipe reduces the coupling between the first cell and the following □ -mode accelerating structure to essentially zero. The phasing between the first cell and the acceleration section is adjustable.

Table 5-3 Cathode cell characteristics

Frequency	1.30	GHz
Q_0	22000	
Peak Power	752	kW
Peak $E_{cathode}$	64	MV/m
Peak E_{wall}	87	MV/m
Peak wall magnetic field	71	kA/m
Transit time factor (T), β=1	0.821	
Z_{shunt}	7.19	Mohm
Z_{shunt} T^2	4.84	Mohm

The 3-cell Acceleration Section

The cathode cell is followed by a 3-cell accelerating structure of conventional design. Each 1.3 GHz cavity (11.54 cm between cavity centers) supports a peak axial E-field of 40 MV/m to accelerate the electron bunch to a final energy of 10.2 MeV.

The coupling between the three accelerating cells is small, and each cell is independently driven through two waveguide ports, to reduce the peak power density at each drive port, and to eliminate any transverse dipole moment.

Cavities – RF Drive

The four cavities in the photoinjector will be driven independently. Each cavity will be driven from a pair of slot waveguide couplers to eliminate any tendency of exciting transverse dipole modes in the cavities, and to reduce the incident power density on the rf windows and coupling apertures. Figure 5-5 shows a MAFIA mesh of the first cell with the waveguide-driven slot coupler, in quarter-cut symmetry

Table 5-4 lists a summary of the characteristics of each of the three identical accelerating cells.

Table 5-4 Characteristics of rf gun accelerating cells

Frequency	1.30	GHz
Q_0	29000	
Peak rms Power	1334	kW
Peak E_{axis}	40	MV/m
Peak E_{wall}	49.4	MV/m
Transit time factor (T), β=1	.689	
Z_{sh} , each cell	6.09	Mohm
$Z_{sh}T^2$, each cell	2.89	Mohm
Energy gain/cavity	2.77	MeV

.

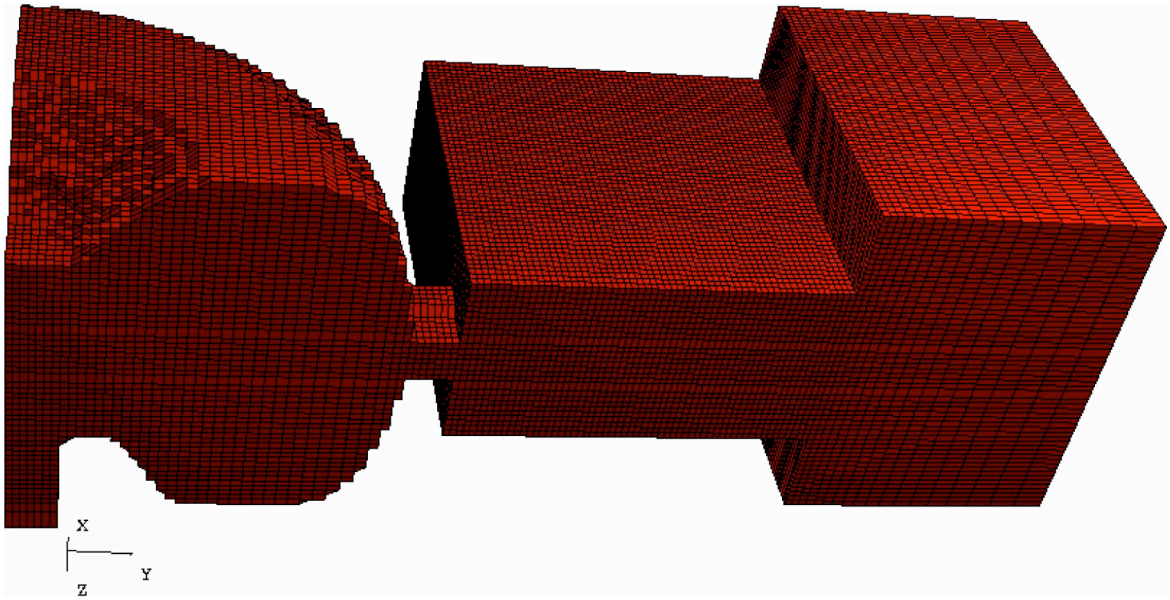

Figure 5-5 3-D model of rf cell, coupler, and input waveguide (MAFIA).

A full-height waveguide feeds a quarter-wavelength of half-height waveguide, which fits in between the solenoids, and which in turn drives the coupling slot itself. Each of the two coupling slots, located on the equator of the cavities, has a cross-sectional area of approximately 4 cm^2, giving critical coupling, and is 1 cm long in order to provide space for the water cooling passages incorporated into the wall.

The cross-sectional profile of the coupling slot is a dumbbell shape, with the radii of the ends of the profile 0.75 cm, and with the centers of the two ends separated by 2.5 cm. This profile will minimize peak magnetic fields and therefore peak surface power dissipation that usually occurs at the ends of slot couplers.

Each of the four cells will be independently driven from separate klystrons, through circulators and power dividers into each of the two drive ports. The phasing of the rf drive to each of the three accelerating cavities is adjusted for π-mode operation. The small iris diameter (2 cm) effectively decouples the cavities from each other. The impact of transverse dipole wakefield from these irises upon emittance growth and energy spread is assessed.

The phasing between the first cell and the three acceleration cells is variable, and due to the long exit snout of the first cell, the coupling to the accelerating cells is effectively zero. In addition, the phasing of the laser pulse to the photocathode is also independently adjustable, with the electron emission occurring at a rather early (20°) phase relative to the rf phase in the first cell. The bunch passes through the centers of the three accelerating cells on the rf crest.

Cavity Wall Power Density and RF Drive Waveform

The wall power density is of critical interest in this high duty factor injector. Nominally, the repetition rate is 10 kHz with an rf pulse length of 5 microseconds, for a macro duty factor of 5%. This is much higher than any existing photoinjector and results in a high average power to the cavities.

The pulse length of 5 microseconds is only 50% greater than the 1/*e* cavity filling time of 3.4 microseconds. If the accelerating cavity is driven at its asymptotic power of 1.33 MW, the gradient will have risen to only 77% of full gradient at 5 microseconds. To bring the cavity to full gradient in 1.5 filling times, the drive voltage must be increased by 30%, corresponding to a drive power increase of 69%, or, for the accelerating cavities, about 2.5 MW.

The envelope of the rf waveform in the cavities will not be a square wave, but will clearly show the exponential rise and fall during and after the pulse. This waveform will actually reduce the average thermal power in the cavities.

If the cavities are overpowered by 69% for 5 microseconds and then allowed to decay after the 20 psec beam pulse, the actual thermal load is only 80% of an equivalent thermal load of a 5 microsecond square waveform in the cavities.

The average thermal power can be further reduced by actively removing the power from the cavities by reversing the drive phase of the applied power, which will remove the stored energy over a 2 microsecond period and deposit it in the dummy load associated with the circulator.

If the stored energy is actively removed from the cavity as described above, the total thermal power is reduced to only 59% of the equivalent square wave rf pulse in the cavities. Under the assumption that the actual cavity Q_0 is 85% of the theoretical copper Q_0, the wall power density savings are significant, with the worst-case wall power density in the first cell decreasing from 116 watts/cm^2 for the square-wave case to 81 watts/cm^2 with active stored energy removal and 85% copper conductivity.

The upper plot of Figure 5-6 shows the cavity voltage waveform for a 5 microsecond pulse and a 3.4 microsecond filling time with unity coupling, overdriven to achieve 100% gradient at 5 microseconds. The lower plot shows the effect of reversing the drive phase at 5 microseconds and continuing the drive for another two microseconds. In this case, the integrated thermal power is only 59% of the square-wave power. Studies show that increasing the coupling, reducing Q_L and the filling time do not significantly lower the average thermal load in the cavity.

The rf gun will require 8.7 MW of peak power, with 1.2 MW for the first cavity, and 2.5 MW for each of the three accelerating cavities. At 5% duty factor, 5 microsecond pulse length at 10 kHz, the average power requirement will be 435 kW, or possibly more, if the phase flip technique of actively removing the stored energy from the cavity is used, where the pulse length may extend to 7 microseconds.

To obtain maximum flexibility for the adjustment of the flat beam parameters, the preferred solution is an arrangement of four independent klystron systems, one for each cavity in the photoinjector. This allows one to take full advantage of fast individual control of each resonator by a digital controller acting directly on a low-power vector modulator, avoiding the use of a high-power rf distribution network with ferrite phase shifters and attenuators.

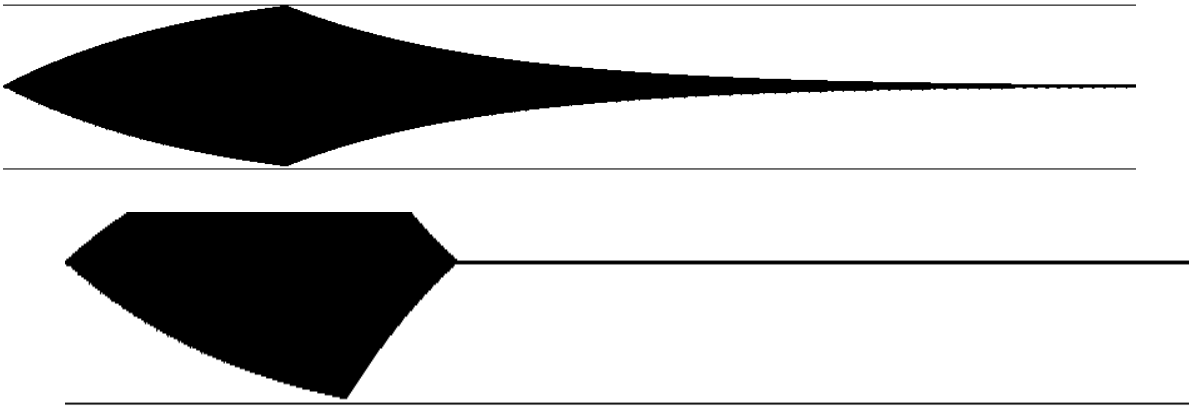

Figure 5-6 Cavity gradient with 5 microsecond rf pulse, 3.4 μs fill time. Top - no active stored energy removal; bottom - active stored energy removal

Mechanical Considerations

The four cavities that comprise the photoinjector will operate at a nominal 5% duty factor, or perhaps even higher. The wall power density will approach 81 watts/cm^2 in certain regions of the OFHC cavity, and will average 38 watts/cm^2 over the entire cavity, which will require careful thermal management, but is within the conservative operating range for room temperature, water-cooled copper structures.

The photoinjector will incorporate water-cooling passages integral to the cavities themselves. ANSYS modeling of the temperature and mechanical stress starts with determining the wall power density with the *e-mag* electromagnetics module, cross-checked with MAFIA simulations to ensure that the wall power density in the vicinity of the drive ports is modeled correctly. Figure 5-7 shows an ANSYS model of an earlier configuration of a 4-cell photoinjector with large drive ports, now replaced with slot couplers, and an initial configuration of integral water-cooling passages.

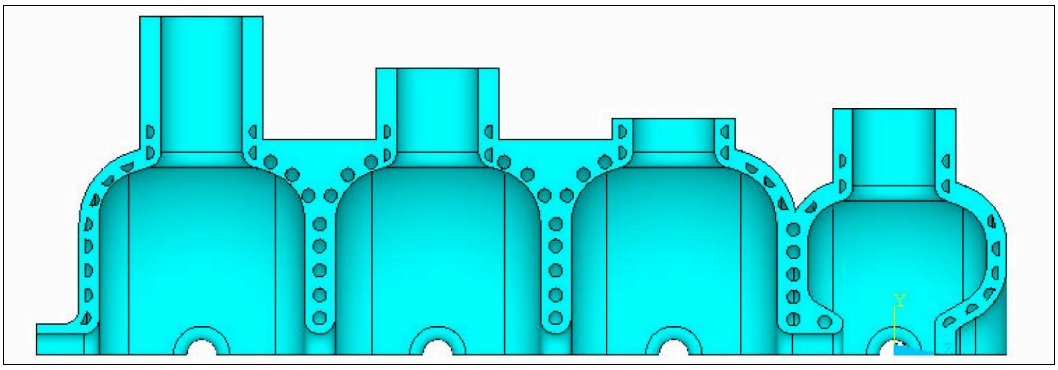

Figure 5-7 ANSYS cavity geometry.

An ANSYS model of the 4-cell cavity has been assembled, and preliminary calculations have been carried out to investigate the temperature rise. Mechanical stress within the cavity structure will be studied in the future.

Figure 5-8 shows the temperature rise with 33 kW dissipated in each cavity. This is 71% of the power that would be dissipated with the active stored energy removal scheme and therefore would show 71% of the expected temperature rise. Subsequent calculations will reflect the revised rf drive geometry and will be renormalized to the expected wall power density.

The photocathode plug will be removable and will be introduced from the photocathode preparation chamber. The high electric fields and high displacement currents in this region will require careful engineering of the cathode assembly to integrate well into the cavity structure, and be compatible with high vacuum requirements and surface preparation methods. In addition, the geometry immediately surrounding the cathode may be modified to produce a small radial focusing field in the first cell.

During rf conditioning of the electron gun, the cathode will be replaced with an un-coated molybdenum plug, so as to avoid contamination or degradation of the surface coating due to vacuum breakdown events. After the gun has been conditioned, the molybdenum plug will be replaced with a fully coated cesium-telluride cathode.

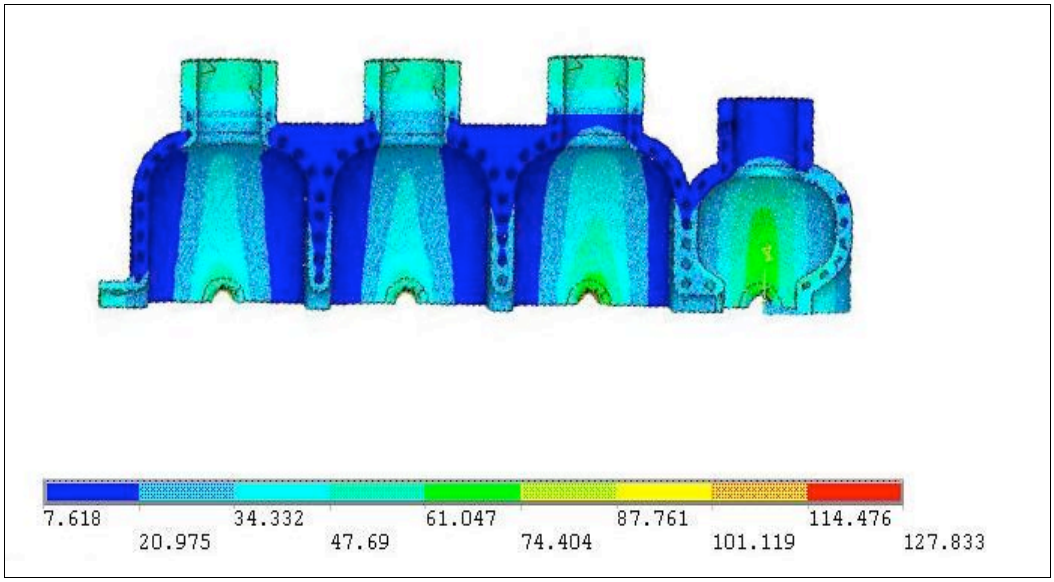

Figure 5-8 ANSYS model of steady-state thermal loading in the rf gun.

Higher Repetition Rates

The total rf power demand (752 + 3 x 1330 = 4742 kW) is large, and at 5% duty factor at a 10 kHz pulse rate approaches a quarter of a megawatt average power needing to be conducted away from the cavity. Operation at a higher pulse rate would require essentially CW operation of the cavities. In this case, the peak fields in the cavities would be reduced and the beam dynamics adjusted accordingly.

FOCUSING SOLENOIDS

The beam will be launched from the cathode immersed in a longitudinal magnetic field, and be focused throughout the 4-cell structure by three or four more solenoids through to the exit. The magnetic field strength on axis at the cathode is adjustable over the 1-1.4 kgauss range to prepare the beam for the flat beam transformer, and to allow for emittance compensation.

Four or five solenoid coils surround the structure, each with a cross section of 5 cm by 5 cm, with a major radius of 13.5 cm. The rf waveguide feeds and other cavity utilities occupy the space between the solenoids. Each solenoid will operate up to an excitation of 20000 ampere-turns, or a current density of about 5100 amps/in^2. With at least a 70% packing factor, this represents a reasonable margin of safety. Figure 5-9 shows five solenoids surrounding a 4-cell structure.

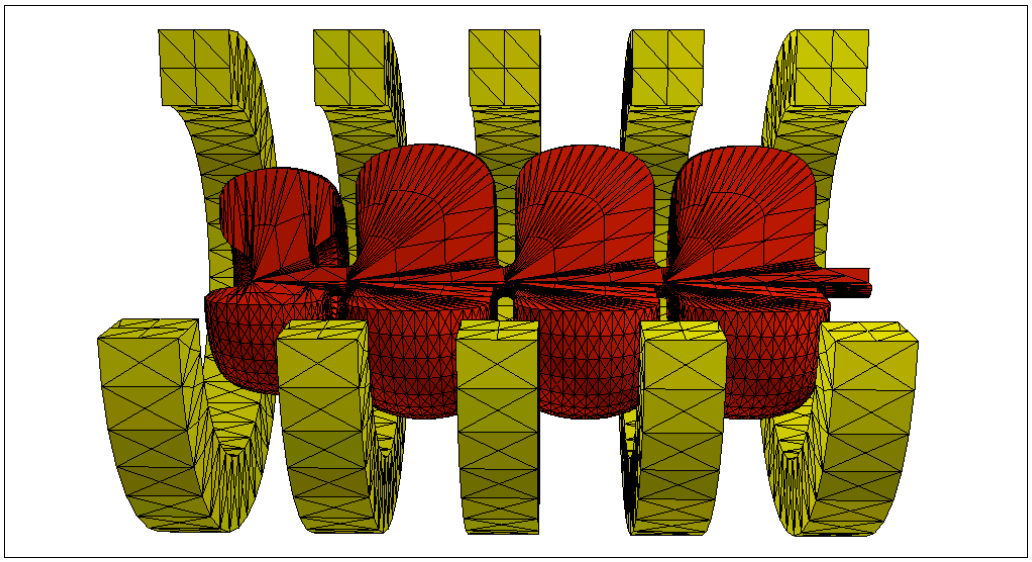

Figure 5-9 MAFIA 3-D model of 4-cell rf gun cavities and solenoid coils. The photocathode is located at the far left.

REFERENCES

[1] J. Yang, *et al.*, 'Experimental Studies of Photocathode RF Gun with Laser Pulse Shaping', to appear in the *Proceedings of the Eighth European Particle Accelerator Conference* (EPAC 2002), Paris, France, 2002.

[2] H. Tomizawa, *et al.*, 'Reduction of electron-Beam Emittance with Shaping Both Spatial and Temporal Profiles of UV Laser Light source for Photo-Cathode RF Gun', to appear in the *Proceedings of the Eighth European Particle Accelerator Conference* (EPAC 2002), Paris, France, 2002.

[3] P. Michelato, *et al.*, 'Thermal Emittance Estimation Using a Time-of-Flight Spectrometer', *Proceedings of the Seventh European Particle Accelerator Conference* (EPAC 2000), Vienna, Austria, 2000.

[4] B. M. Dunham, *et al.*, 'Emittance Measurements for the Illinois/CEBAF Polarized Electron Gun', *Proceedings of the 1995 Particle Accelerator Conference*, (IEEE, New York).

[5] W. Hartung, *et al.*, 'Studies of Photo-Emission and Field Emission in an rf Photo-Injector with a High Quantum Efficiency Photo-Cathode', *Proceeding of the 2001 Particle Accelerator Conference*, (IEEE, New York), 2001.

[6] K. Halbach and R. Holsinger, Particle Accelerators, **3**, 213 (1976).

[7] T. Weiland, *et al.*, *Proceedings of the Linear Accelerator Conference*, SLAC-303, 282 (1986).

[8] ANSYS is a registered trademark of ANSYS, Inc. (www.ansys.com)